Negative refraction in semiconductor metamaterials

ANTHONY J. HOFFMAN[1]*, LEONID ALEKSEYEV[1], SCOTT S. HOWARD[1], KALE J. FRANZ[1], DAN WASSERMAN[1], VIKTOR A. PODOLSKIY[2], EVGENII E. NARIMANOV[1], DEBORAH L. SIVCO[3] AND CLAIRE GMACHL[1]

[1]Department of Electrical Engineering, Princeton University, Princeton, New Jersey 08544, USA
[2]Physics Department, Oregon State University, Corvallis, Oregon 97331, USA
[3]Alcatel-Lucent, Murray Hill, New Jersey 07974, USA
*e-mail: ajhoffma@princeton.edu

Published online: 14 October 2007; doi:10.1038/nmat2033

An optical metamaterial is a composite in which subwavelength features, rather than the constituent materials, control the macroscopic electromagnetic properties of the material. Recently, properly designed metamaterials have garnered much interest because of their unusual interaction with electromagnetic waves[1–3]. Whereas nature seems to have limits on the type of materials that exist, newly invented metamaterials are not bound by such constraints. These newly accessible electromagnetic properties make these materials an excellent platform for demonstrating unusual optical phenomena and unique applications such as subwavelength imaging and planar lens design. 'Negative-index materials', as first proposed, required the permittivity, ε, and permeability, μ, to be simultaneously less than zero, but such materials face limitations. Here, we demonstrate a comparatively low-loss, three-dimensional, all-semiconductor metamaterial that exhibits negative refraction for all incidence angles in the long-wave infrared region and requires only an anisotropic dielectric function with a single resonance. Using reflection and transmission measurements and a comprehensive model of the material, we demonstrate that our material exhibits negative refraction. This is furthermore confirmed through a straightforward beam optics experiment. This work will influence future metamaterial designs and their incorporation into optical semiconductor devices.

Although the concept of negative-index materials (NIMs) has existed for several decades, actual metamaterials with these properties were not fabricated until recently[1–3]. The original proposal and subsequent implementation in the microwave region for a practical NIM consisted of thin wires and split rings producing overlapping electric and magnetic resonances, respectively, to give $\varepsilon, \mu < 0$ (refs 3–5). More recently, new designs that exhibit negative refraction in the near-infrared and optical frequencies have been fabricated and characterized[6–8]. These materials no longer use the aforementioned design; however, they still rely on overlapping resonances in ε and μ. This double-resonance scheme is hindered because design and fabrication can be complicated, the nature of the resonances induces high loss inside the material and the creation of a three-dimensional metamaterial from existing structures is difficult due to limitations in fabrication technology. One strategy to greatly ease design, reduce loss and create bulk-like metamaterials is to create a material with only a single resonance. For these materials however, a second optical characteristic, such as anisotropy or chirality, needs to be used to produce negative refraction, thus distinguishing it from naturally occurring resonant materials[9–12].

To improve on the limitations of double-resonance metamaterials, we demonstrate a semiconductor metamaterial that exhibits negative refraction for all incident angles in the long-wave infrared region of the spectrum. This optically thick material consists of alternating layers of highly doped InGaAs and intrinsic AlInAs and exhibits a strongly anisotropic dielectric function that obviates the need for simultaneously negative electric and magnetic responses. The spectral region of negative refraction has a bandwidth $\geq$27%, and its starting wavelength is controlled by the electron density in the doped layers; for our choice of semiconductor heterostuctures, it can be located anywhere above $\sim$8.8 μm.

In anisotropic materials, the electric-field vector, **E**, and the electric-displacement vector **D**, are not usually parallel. An immediate consequence of this is that the Poynting vector, **S**, which points in the direction of energy flow, and wavevector, **k**, directed along the wavefront normal, need not be parallel. As the boundary conditions at the interface of two materials require only that the tangential component of **k** is conserved, it is possible for the refracted beam to exhibit normal refraction with respect to **k** but negative refraction with respect to **S**. A uniaxial anisotropic material with $\varepsilon_{\parallel} > 0$ and $\varepsilon_{\perp} < 0$, where $\varepsilon_{\perp}$ and $\varepsilon_{\parallel}$ are the components of the permittivity relative to the surface of the material (see Fig. 1a inset for definition), will exhibit this behaviour for the transverse magnetic polarization for all incidence angles. As the transverse electric polarization does not experience anisotropy, both **k** and **S** refract normally[9]. Such a material is exceptionally different from natural anisotropic materials that rarely exhibit negative refraction and if they do, do so for only a small range of incidence angles[13].

To demonstrate negative refraction at infrared wavelengths, we designed and fabricated four samples composed of interleaved 80 nm layers of $In_{0.53}Ga_{0.47}As$ and $Al_{0.48}In_{0.52}As$. The layers, approximately 8.1 μm thick, were grown by molecular beam epitaxy on lattice-matched InP substrates. The InGaAs layers were uniformly doped, at different densities for each sample,

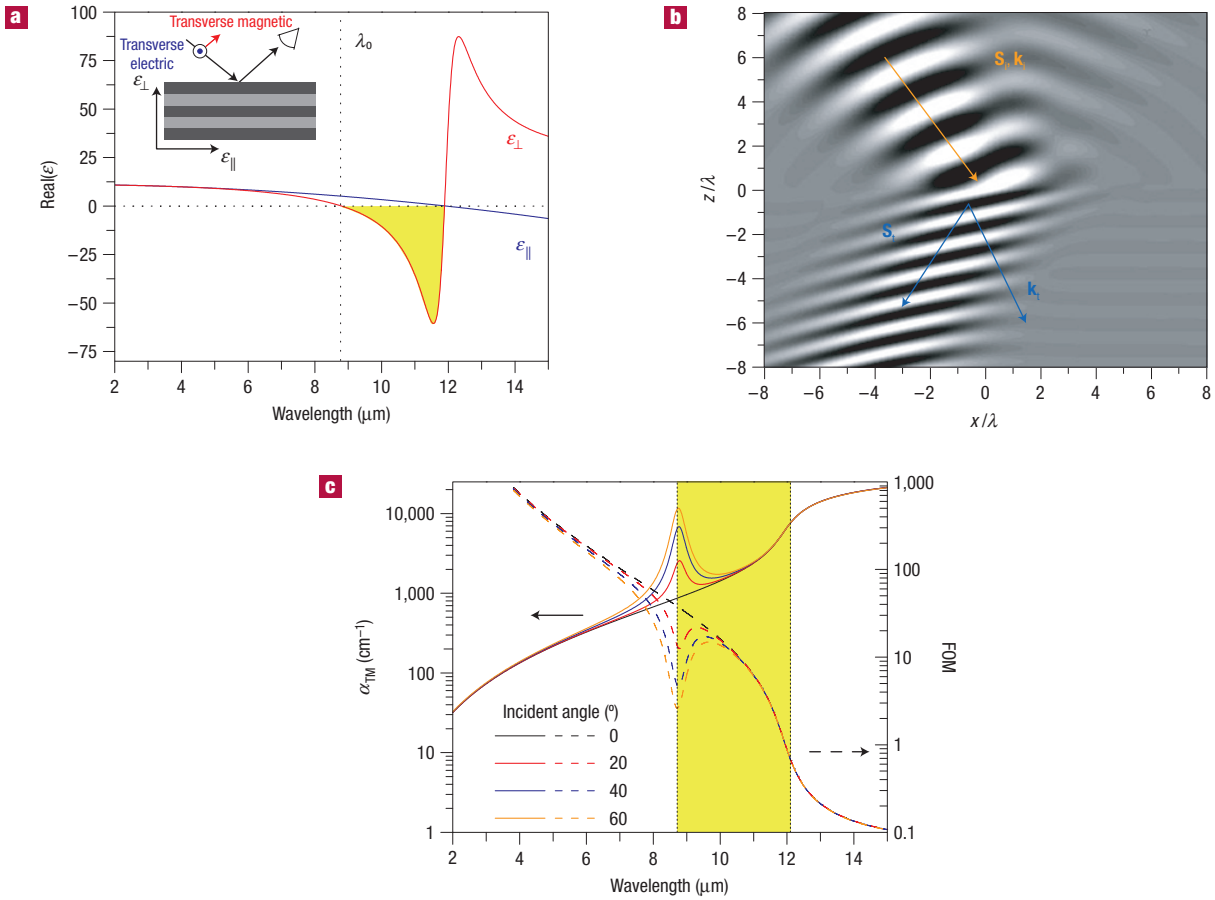

Figure 1 Calculated dielectric function and beam refraction. a, Dielectric function, $\varepsilon_\perp$ and $\varepsilon_\parallel$ of an n^+–i–n^+ heterostructure calculated using the effective medium theory and $n_d = 7.5 \times 10^{18}$ cm^{-3}. The inset shows the relative orientation of the dielectric function ($\varepsilon_\perp$ and $\varepsilon_\parallel$), the electric-field vectors (transverse electric, transverse magnetic) and the layered structure. **b**, Full numerical calculations demonstrating negative refraction of a monochromatic transverse-magnetic-polarized gaussian beam across an air–metamaterial interface. **c**, Calculations of the absorption coefficient for the transverse magnetic polarization, α_{TM}, and the figure of merit, FOM, as a function of wavelength for a metamaterial with the dielectric function shown in **a**. The portion shaded in yellow indicates the spectral region where the metamaterial exhibits negative refraction.

to provide a plasma resonance of free carriers. Figure 1a shows the calculated components of the dielectric function for a metamaterial with a free-electron density, n_d, of 7.5×10^{18} cm^{-3}. The spectral region where the metamaterial will exhibit negative refraction is indicated by the shaded yellow region. The onset of negative refraction occurs at λ_o, or the critical wavelength, when $\varepsilon_\perp = 0$. Figure 1b shows full numerical calculations for the refraction of a monochromatic transverse-magnetic-polarized gaussian beam across the air–metamaterial interface in the negative-refraction regime. The absorption coefficient for the transverse magnetic polarization, α_{TM}, and the figure of merit (FOM), $\mathrm{FOM} = \mathrm{Re}(k_\perp)/\mathrm{Im}(k_\perp)$, were calculated using the effective medium approximation. The FOM is an accepted value for characterizing materials that exhibit negative refraction and the presented metamaterial improves on this parameter significantly[14]. Figure 1c shows both α_{TM} and FOM as a function of wavelength at several incident angles for a metamaterial with a permittivity tensor as shown in Fig. 1a.

For each sample, the free-carrier density of the InGaAs layers, n_d, was extracted from transmission measurements (see Supplementary Information for details). The so-extracted densities for our samples are 3.4×10^{18} cm^{-3}, 5.7×10^{18} cm^{-3}, 7.1×10^{18} cm^{-3} and 7.5×10^{18} cm^{-3}, resulting in critical wavelengths of 13.1, 10.1, 9.1 and 8.8 μm, respectively. Table 1 summarizes n_d and λ_o for our metamaterial samples. We also grew a control sample which is composed of a single ~4.7-μm-thick InGaAs layer doped 5.8×10^{18} cm^{-3}. This sample and a low-doped InP substrate serve as isotropic controls (results in Supplementary Information).

Table 1 Summary of the samples of the study. The spectral location of the transition from positive to negative refraction, λ_o, is reported as a function of the free-carrier density, n_d, in the InGaAs layers. The values reported for n_d were extracted from the experimental measurements as outlined in the Supplementary Information.

Sample	n_d (1×10^{18} cm^{-3})	λ_o (μm)
A	3.4	13.1
B	5.7	10.1
C	7.1	9.1
D	7.5	8.8

The onset of negative refraction strongly influences the macroscopic electromagnetic properties of the material. To observe

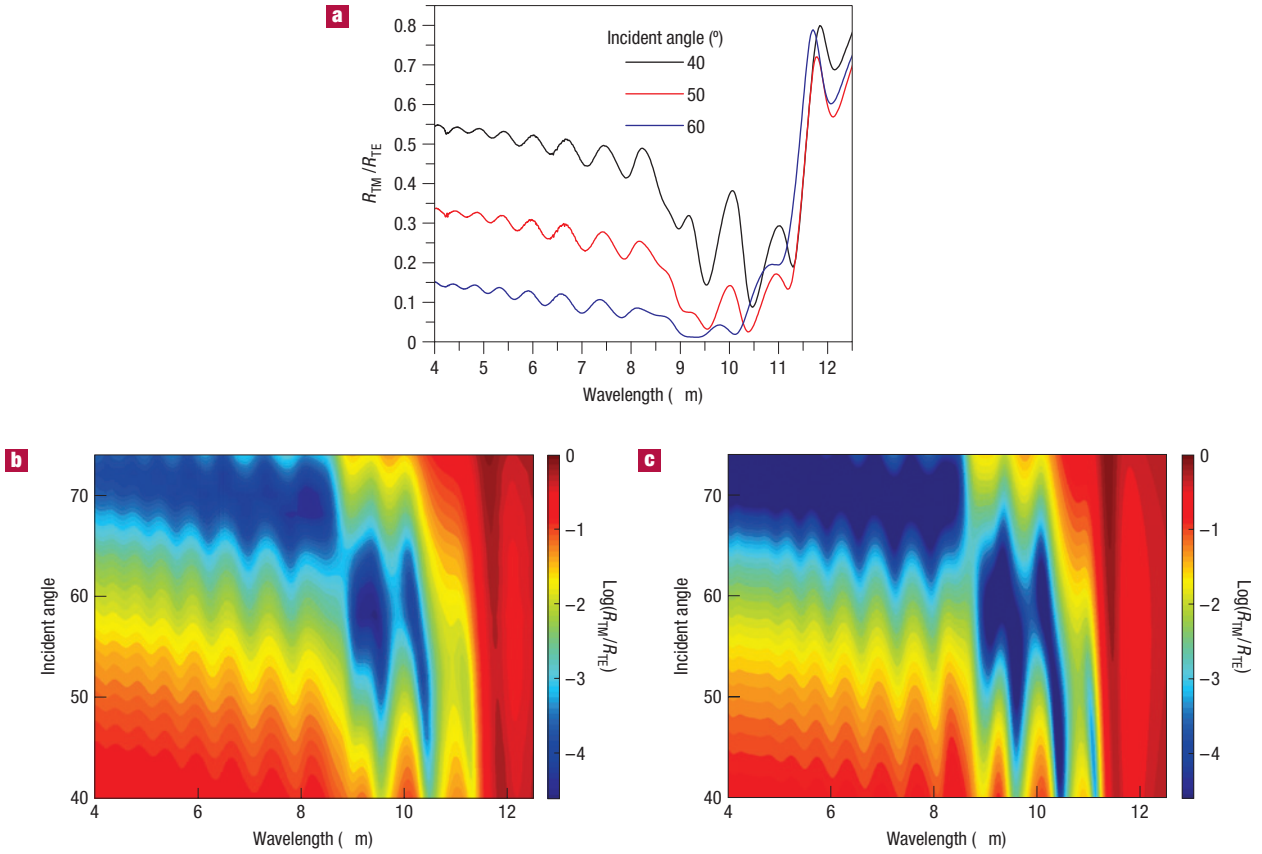

Figure 2 Experimental results and theoretical calculations of reflectance. **a**, Measured ratio of transverse magnetic/transverse electric reflectance, R_{TM}/R_{TE}, of sample D with $n_d = 7.5 \times 10^{18}$ cm^{-3} and an epitaxial layer thickness of 8.08 μm for select incident angles. **b**, Measured R_{TM}/R_{TE} versus wavelength and incident angle. The plot is composed of many curves such as those shown in **a**. The reflectance ratio is plotted on a logarithmic scale. The discontinuity at 8.8 μm is due to a discontinuity in the transverse magnetic reflectance and marks the transition into negative refraction. **c**, Theoretical reflectance calculations of **b** for comparison using only the doping density and sample thickness.

the transition, we conducted reflection and transmission measurements (transmission measurements are shown in Supplementary Information) as a function of polarization, incident angle and wavelength. A Fourier-transform infrared spectrometer, ZnSe or Ge lenses, and a liquid-nitrogen-cooled mercury–cadmium–telluride detector (with a cutoff wavelength of ~15 μm) were used for all measurements. The light from the Fourier-transform infrared spectrometer source was focused onto a small spot, ~250 μm, at the centre of the sample, which was typically a full quarter of a 2 inch wafer. The large sample reflected or transmitted the entire beam, despite the beam's elliptical profile on the sample surface due to an oblique incident angle, and the light was collected on the detector. Data were averaged over 400 scans using a spectral resolution of 4 cm^{-1}. Experimental error is 1–5% of the absolute measurement value, which is typical for this type of Fourier-transform infrared spectroscopy experiment.

For the reflection measurements, the specular reflection for light incident on the epitaxial layer was measured from 40 to 74° in 2° increments for each metamaterial sample and the high-doped control. The data are analysed as the ratio of transverse magnetic to transverse electric reflectance with the purpose of minimizing environmental fluctuations. Figure 2a shows curves for select incident angles of the experimental reflection measurements for sample D, $n_d = 7.5 \times 10^{18}$ cm^{-3}. Figure 2b shows a log-scale colour plot versus incident angle and wavelength composed of several curves such as those shown in Fig. 2a. The corresponding theoretical calculations, which use only the sample thickness and n_d, are shown in Fig. 2c. The results were obtained using an anisotropic transfer matrix approach[15]. There is excellent agreement between experiment and theory. The apparent step around 8.8 μm is due to a discontinuity in the Brewster angle (transverse magnetic polarization) as predicted by theory and occurs in the expected spectral range where $\varepsilon_\perp \approx 0$; the fringes are due to interference effects across the epitaxial layer. The three other metamaterial samples, A–C, also exhibit such discontinuities at their respective critical wavelengths and agree well with theoretical calculations. Similar analysis of the isotropic, highly doped control sample shows no discontinuity in the Brewster angle with wavelength (data shown in Supplementary Information).

We determined the bandwidth of the spectral region that exhibits negative refraction. The short-wavelength limit of the region is marked by the discontinuity of the Brewster angle and the long-wavelength limit is marked by a large increase in the reflectivity. This increase, which approaches unity for long wavelengths, is due to both the real parts of $\varepsilon_\parallel$ and $\varepsilon_\perp$ approaching 0 (see Fig. 1a, $\lambda = 11.8$ μm) and their growing imaginary parts. We use 50% transverse electric reflectivity for an incident angle of 40° to mark the end of the region. The bandwidth for sample D, about the central wavelength of the region, is greater than 27%.

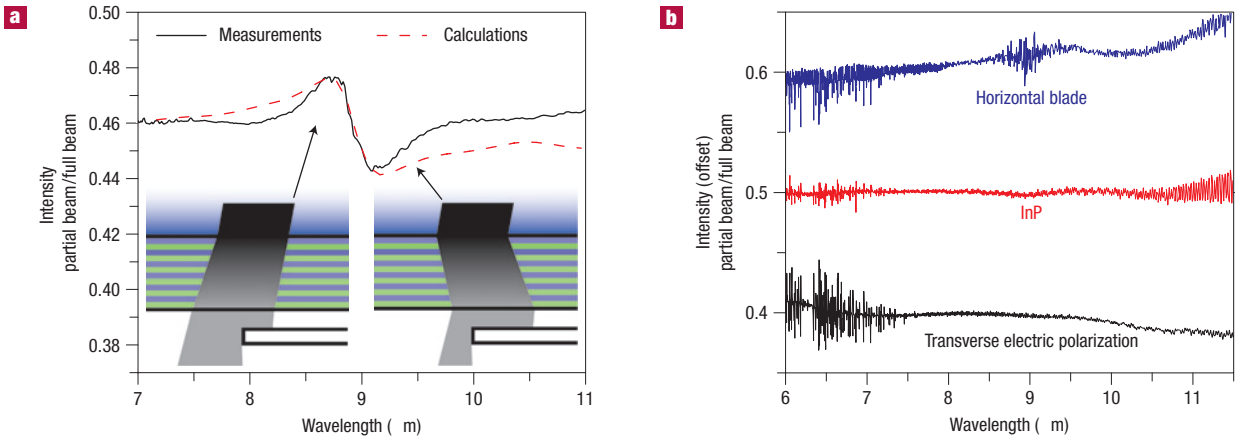

Figure 3 Experiment demonstrating the transition from positive to negative refraction. a, Spectra of the ratio of a partially blocked beam to an unblocked beam for sample D. The insets show the configuration for the measurement. Transverse-magnetic-polarized light was weakly focused onto the InP substrate with an incident angle of 50°. The peak for $\lambda < \lambda_0$ occurs because the transmitted beam shifts away from the blade and relatively more light is measured. The dip for $\lambda > \lambda_0$ arises because the beam shifts behind the blade and relatively less light is transmitted. The dashed line represents the calculated behaviour as modelled in a straightforward simulation using Fourier optics. **b**, Spectra of control measurements for transverse-electric-polarized light and sample D; transverse-magnetic-polarized light and InP substrate; and transverse-magnetic-polarized light when the blade is rotated 90°, about the surface normal, from the orientation shown in **a**. The bottom curves do not show the feature present in **a** because they lack a strongly wavelength-dependent angle of refraction. The top curve does not exhibit the feature because the incident angle, nearly 0°, is insufficient to cause a substantial beam shift.

The remaining metamaterial samples exhibit values of 29%, 29% and 28% for samples A, B and C respectively.

To characterize the optical loss of the metamaterials, we used both the transmission and reflection measurements to estimate the absorption coefficient for the transverse magnetic polarization, α_{TM}, at the peak-transmission wavelength in the negative-refraction regime, that is, ~9.9 μm for sample D. The measured losses were compared with theoretical values obtained using an anisotropic transfer matrix. For both experiment and theory, $\alpha_{TM} \approx -\ln(T_{TM}/(1-R_{TM}))/L$, where T_{TM} and R_{TM} are the transverse magnetic transmittance and reflectance respectively, and L is the thickness of the metamaterial. For sample D, the measured loss for an incident angle of 40° is 1,800 cm^{-1} and increases approximately linearly with increasing incident angle to 2,100 cm^{-1} at 60°. The measured loss is approximately 15% greater than the theoretical prediction.

We also carried out a series of geometric optics experiments to demonstrate the change from positive refraction to negative refraction for macroscopic beams around λ_0. For the measurements, broadband transverse-magnetic-polarized light from the Fourier-transform infrared source was weakly focused onto the sample to a ~250-μm-diameter spot using a 6-inch-focal-length ZnSe meniscus lens with a mean incident angle, θ_i, of 50° and a full angular spread, $\Delta\theta$, of about 6°. To distinguish between positive and negative refraction, we first collect transverse magnetic transmission data of the full beam as a function of wavelength. We then block half of the transmitted beam with a blade a small distance away from the sample, as shown in Fig. 3a, and again measure the spectrum. The ratio of the two measurements, partially blocked to full beam, is shown in Fig. 3a and shows the relative amount of light that was measured when the blade was in place. For wavelengths with positive refraction (left inset of Fig. 3a), the beam shifts slightly away from the blade edge, thus allowing more light to transmit past the blade, resulting in a peak. For wavelengths with negative refraction (right inset of Fig. 3a), the beam shifts slightly behind the blade and results in a dip. Calculations using Fourier optics methods were used with the theoretical model of the metamaterial to simulate the experiment. The results of these calculations are shown by the dashed red curve. We also carried out numerous control measurements: switching the blade to the other side of the sample while keeping the incidence angle fixed reverses the dip and peak; likewise, keeping the blade on the same side and changing θ_i to $-\theta_i$ has the same effect. The transverse electric polarization with metamaterial samples and the transverse magnetic polarization with an InP control sample (both shown in Fig. 3b) do not possess features similar to Fig. 3a because the materials lack the quickly changing angle of refraction with wavelength. Finally, the blade edge set perpendicular to the axis of rotation of the sample (rotated 90° with respect to Fig. 3a) also does not show intensity variation with wavelength because the incident angle, which affects the magnitude of the shift, is nearly 0°. The relative increase and decrease (peak and dip) in the graph in Fig. 3a is a macroscopic manifestation of the transition from positive to negative refraction of our material.

In summary, using reflection and transmission measurements and geometric beam optics, we have demonstrated a new class of metamaterials that exhibit negative refraction across wide wavelength ranges in the long-wave infrared region. The metamaterial design is unique in that it relies on an anisotropic dielectric function, instead of overlapping electric and magnetic resonances, which makes it straightforward to design and comparatively low-loss. Furthermore, it is all-semiconductor, planar, three-dimensional in structure and requires no further nanofabrication beyond the initial growth. Such a metamaterial has great potential for waveguiding and imaging applications.

Received 2 July 2007; accepted 6 September 2007; published 14 October 2007.

References

1. Veselago, V. G. Electrodynamics of substances with simultaneously negative values of sigma and mu. *Sov. Phys. Usp.* **10**, 509 (1968).
2. Smith, D. R., Padilla, W. J., Vier, D. C., Nemat-Nasser, S. C. & Schultz, S. Composite medium with simultaneously negative permeability and permittivity. *Phys. Rev. Lett.* **84**, 4184–4187 (2000).
3. Shelby, R. A., Smith, D. R. & Schultz, S. Experimental verification of a negative index of refraction. *Science* **292**, 77–79 (2001).
4. Moser, H. O., Casse, B. D. F., Wilhelmi, O. & Saw, B. T. Terahertz response of a microfabricated rod-split-ring-resonator electromagnetic metamaterial. *Phys. Rev. Lett.* **94**, 063901 (2005).

5. Koschny, T., Kafesaki, M., Economou, E. N. & Soukoulis, C. M. Effective medium theory of left-handed materials. *Phys. Rev. Lett.* **93**, 107402 (2004).
6. Shalaev, V. M. *et al.* Negative index of refraction in optical metamaterials. *Opt. Lett.* **30**, 3356–3358 (2005).
7. Zhang, S. *et al.* Experimental demonstration of near-infrared negative-index metamaterials. *Phys. Rev. Lett.* **95**, 137404 (2005).
8. Zhang, S. *et al.* Demonstration of metal-dielectric negative-index metamaterials with improved performance at optical frequencies. *J. Opt. Soc. Am. B* **23**, 434–438 (2006).
9. Podolskiy, V. A. & Narimanov, E. E. Strongly anisotropic waveguide as a nonmagnetic left-handed system. *Phys. Rev. B* **71**, 201101 (2005).
10. Pendry, J. B. A chiral route to negative refraction. *Science* **306**, 1353–1355 (2004).
11. Alu, A. & Engheta, N. Optical nanotransmission lines: Synthesis of planar left-handed metamaterials in the infrared and visible regimes. *J. Opt. Soc. Am. B* **23**, 571–583 (2006).
12. Ivanov, O. V. & Sementsov, D. I. Light propagation in stratified chiral media. The 4 × 4 matrix method. *Crystallogr. Rep.* **45**, 487–492 (2000).
13. Grzegorczyk, T. M., Nikku, M., Chen, X. D., Wu, B. I. & Kong, J. A. Refraction laws for anisotropic media and their application to left-handed metamaterials. *IEEE Trans. Microw. Theory Tech.* **53**, 1443–1450 (2005).
14. Shalaev, V. M. Optical negative-index metamaterials. *Nature Photon.* **1**, 41–48 (2007).
15. Berreman, D. W. Optics in stratified and anisotropic media: 4 × 4-matrix formulation. *J. Opt. Soc. Am.* **62**, 502–510 (1972).

Acknowledgements

The authors would like to thank PRISM, PCCM MRSEC, MIRTHE (NSF-ERC) and ARO-MURI for support of this project. In addition, we would like to thank Z. Jacob for useful discussions.
Correspondence and requests for materials should be addressed to A.J.H.
Supplementary Information accompanies this paper on www.nature.com/naturematerials.